THIRTEENTH EUROPEAN ROTORCRAFT FORUM

2-16

Paper No. 87

THE ACTUATOR DISC EDGE SINGULARITY: THE KEY TO A REVISED ACTUATOR DISC CONCEPT AND MOMENTUM THEORY

Ir. G.A.M. van Kuik

TECHNICAL UNIVERSITY EINDHOVEN
FACULTY OF PHYSICS
WIND ENERGY GROUP

September 8-11, 1987

ARLES, FRANCE

ASSOCIATION AERONAUTIQUE ET ASTRONAUTIQUE DE FRANCE

THE ACTUATOR DISC EDGE SINGULARITY
THE KEY TO A REVISED ACTUATOR DISC CONCEPT
AND MOMENTUM THEORY

G.A.M. van Kuik
The Wind Energy Group of the Technical University Eindhoven

1. Introduction

Since the beginning of rotor aerodynamics the actuator disc momentum theory occupies a prominant place in almost any textbook on this subject. Specially in axial flow the theory provides an easy and rather accurate performance prediction. The results first obtained by Lanchester (ref. 1) for the induced power of a hovering rotor and the maximum power of a wind turbine are still used as guidelines for complicated calculations. On the other hand, experimental results for propellers are known to deviate systematically (some 10%) from the momentum theory results. This is commonly attributed to the differences between a real rotor and an actuator disc. However, some actuator disc- and actuator strip (the 2-dimensional version) experiments are described in literature, showing the same deviations from momentum theory results. Therefore, apart from the question how representative an actuator disc is for a real rotor, the actuator disc concept itself may be inadequate. This problem is the subject of the work describe here. It will be shown that the classical actuator disc concept ignores discrete forces resulting from a flow singularity at the edge of the disc. The (extended) momentum theory, applied to this actuator strip model, shows a shift of the results towards the experimental data, and for the static case (hover) even a quantitative agreement is obtained.

2. Analysis of experimental results

The general behaviour of rotors in axial flow is determined by the undisturbed wind speed (with respect to the rotor) u_0 and the axial thrust T as independent variables, with the average induced velocity at the rotor disc $u_{i,d}$ as dependent

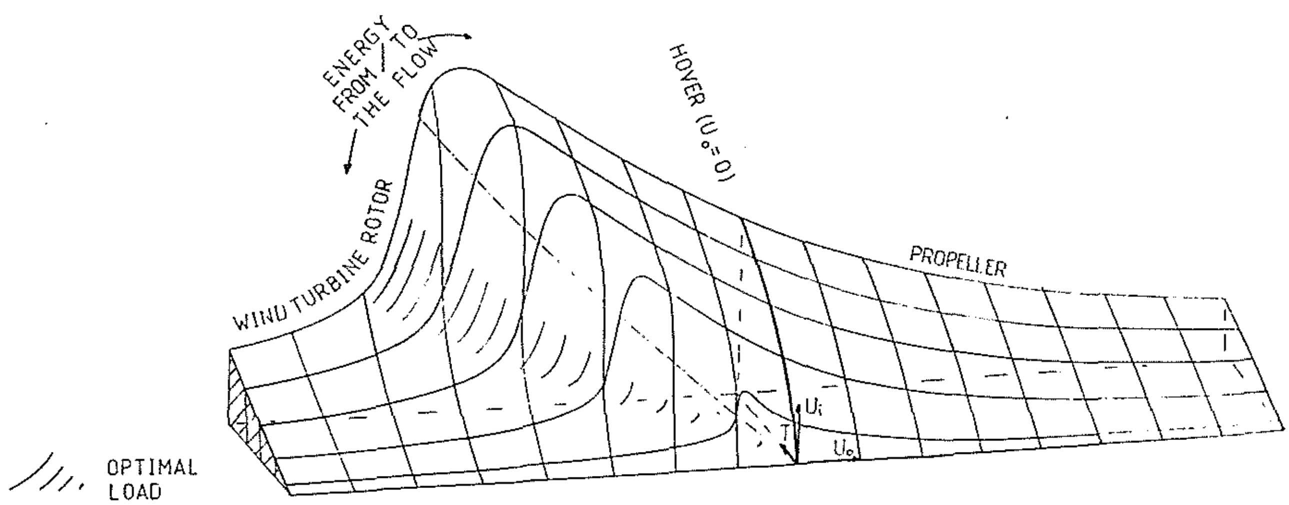

Fig. 1:
A survey of all axial flow states of a rotor: the induced velocity at the rotor disc (u_i) as a function of the independent variables thrust (T) and undisturbed wind speed (u_0).

variable. For propellers and helicopters in steady axial flight, T = constant and an u_0 versus $u_{i,d}$ graph is practical to show results; for wind turbines u_0 is assumed to be steady, and T is the design parameter leading to a T versus $u_{i,d}$ graph. Therefore the comparison of both rotor flow states is not too obvious. Fig. 1 shows a 3-D survey of $u_{i,d}$ as a function of T and u_0. The severe non-linear dependence of $u_{i,d}$ on both T and u_0 for optimally loaded wind turbines is striking: this non-linearity is even stronger than in hover. Fig. 2 shows a comparison of momentum theory and experiments, all referred to a constant T. The over-estimation of $u_{i,d}$ in the wind turbine state and the under-estimation in the propeller state both result in the same phenomenon: the average velocity $|u_d|$ through the rotor disc is always higher than expected ($|u_d| = |u_0+u_{i,d}|$). This implies that in all rotor flow states, where momentum theory provides results, a higher mass flow through the rotor is observed than expected by momentum theory.

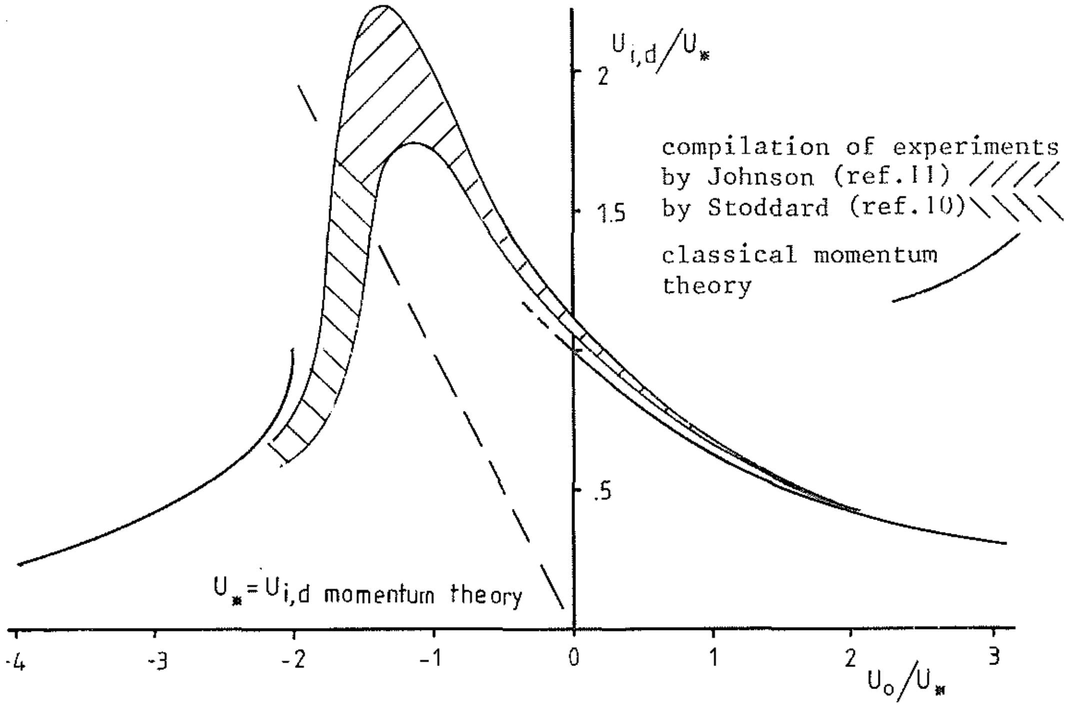

Fig. 2:
The systematic deviation of experimental results from classical momentum theory results.

The same evidence is given by two 2-D actuator strip results of Greenberg & Lee (ref. 2). They performed a 2-D experiment in a shallow water tank (shallow enough to ignore the third dimension): they simulated a line momentum source by an array of closely spaced nozzles, injecting high-velocity, turbulent, incompressible jets into the flow.
By rapid mixing of the jets, and tuning of the nozzles in order to have a negligible mass injection combined with a high momentum, this arrangement is to be considered as an actuator strip with constant load. The ambient velocity was zero, so the hover results should be obtained. Fig. 3 gives these results: the ratio $u_{i,d}/(u_{i,d})_{\text{momentum theory}}$ varies from ~.96 to ~1.12, depending on number of nozzles, flow rate, etc., and on the jet Reynolds number. The highest Reynolds number gives the ratio

~1.12. Also shown in fig. 3 are the computed results of Greenberg & Lee.
These are obtained by initially assuming a shape and strength of the vortex sheets, emanating from the strip edges, and by adjusting these iteratively until the kinematic boundary condition (the vortex sheet to be a streamline) and the dynamic boundary condition (no pressure jump across the vortex sheet) are satisfied. These results agree with the experimental data of fig. 2 and 3. Moreover, the 2-D calculated results are identical to those of similar 3-D calculations of Greenberg (ref. 3). The conclusion seems inevitable: it is not so that the experiments are too far from the ideal actuator disc concept, but this concept is too far from the real physical situation and even from a physical actuator strip.

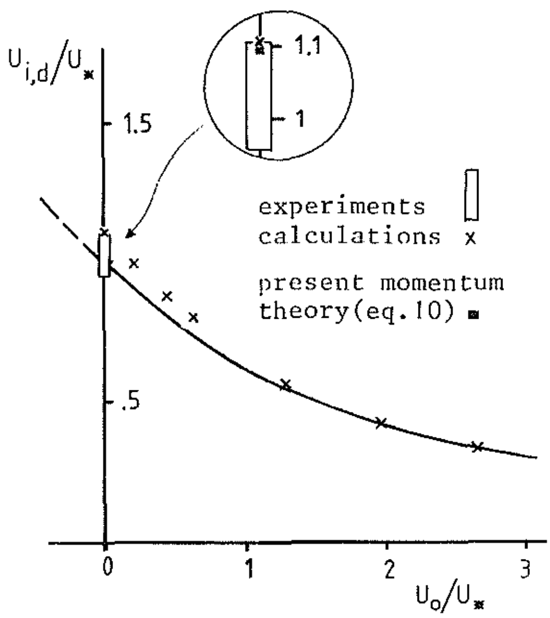

Fig. 3: Experimental and calculated actuator strip results of Greenberg & Lee (ref.2), compared with classical and present momentum theory.

3. The force distribution on an actuator strip

The actuator disc and strip are mathematical limit representations of real rotors. The only physical property which is left is the force field exerted by the rotor to the flow. Therefore it may be useful to reverse the conventional way of thinking in incompressible fluid dynamics: no determination of forces as result of pressure integrations, once the kinematical problem has been solved, but determination of the kinematics of the flow when a specified force field is applied. The Euler equation provides this opportunity by the force density term $\underline{f}$, the dimension of which is N/m^3:*)

$$\rho \frac{\partial \underline{v}}{\partial t} + \underline{\nabla} H = \underline{f} + \rho \ (\underline{v} \wedge \underline{\omega}) \qquad (1)$$

*) Surface forces (N/m^2) are denoted by $\underset{\sim}{F}$, line forces (N/m) by $\underline{F}$.

H is the Bernoulli constant ($p+\frac{1}{2}\rho\underline{v}.\underline{v}$), ρ the specific mass and $\underline{v}$, $\underline{\omega}$ the velocity. resp. vorticity vector. The rotation of (1) gives:

$$\frac{1}{\rho}\,\underline{\nabla}\wedge\underline{f} = -\,\underline{\nabla}\wedge(\underline{v}\wedge\underline{\omega}) + \frac{\partial\underline{\omega}}{\partial t}$$

$$= \frac{D\underline{\omega}}{Dt} \qquad (2)$$

showing that only the rotation of $\underline{f}$ determines the production of vorticity, even in unsteady flows. For actuator strips with a constant, normal load, $\underline{\nabla}x\underline{f} \neq 0$ only at the edges, so attention is focussed to the flow field in a circle (radius r) around the edge, with lim $r\to 0$. The velocity induced by the vortex sheet of the other edge, plus the undisturbed parallel flow, is represented by a local parallel flow. In this way the problem is simplified to the determination of the flow in the neighbourhood of an half-infinite actuator strip edge with constant, normal load F, placed in a parallel flow u_0, fig. 4. This parallel flow u_0 may be zero; if at the edge the velocity induced by the far field vorticity is equal but opposite to the undisturbed parallel flow, the local "ambient" flow is zero. For this situation an exact solution of the flow is obtained, see the appendix. This solution is an instationary one: a discrete vortex is generated at the edge, growing linearly in time:

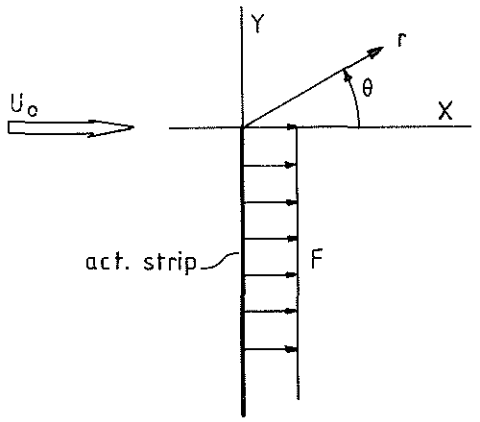

Fig. 4: The half-infinite actuator strip in a parallel flow $\underline{u}_0$.

$$\left.\begin{aligned} \Gamma_{r=0} &= \frac{F}{\rho}\,t \\ \underline{v} = \underline{e}_\theta\, v &= \underline{e}_\theta\,\frac{F}{\rho}\,\frac{t}{2\pi r} \end{aligned}\right\} \qquad (3)$$

The interpretation of (3) is straightforward: as at the *edge* $\underline{v}=0$, the increasing amount of vorticity, determined by (2), cannot be transported from the edge, so accumulates at r=0. A necessary unsteady flow is the result.
This solution is not as hypothetically as it seems: in the rotor performance diagram of fig. 2, the average velocity through the rotor is zero at the dashed line (auto rotation). Near this flow sate, at a somewhat lower negative u_0, the average velocity is non-zero, but the velocity at the outer part will be approximately zero. This situation, with the highest induced power, resembles the flow problem treated here: as the average velocity is zero at the tips, the vorticity cannot be transported downstream, so increases, remaining on the same position; consequently the velocity induced at the vortex ring itself

increases, leading to a non-zero velocity which transports the vorticity away. Then the process starts again: a vortex ring, initially stable, grows in strength and blows itself away.
This behaviour at the vortex ring state, is clearly visualized in the NLR*)-film: "The flow through a helicopter rotor", made in 1950.
The semi-infinite actuator strip with non-zero $\underline{u}_0$ is also analysed in the appendix. An exact solution is not obtained, but the type of flow singularity is determined: at the edge a steady, discrete vortex Γ must be present, carrying a discrete force $\underline{F}_e$. This force $\underline{F}_e$ is additional to the constant load on the strip itself: the force distribution is:

$$\begin{aligned} \underline{F} &= \underline{e}_x\, F = \underline{e}_x\, \Delta p && y \le 0 \\ \underline{F}_e &= \underline{e}_n\, \underline{F}_e = -\rho\, \underline{V} \wedge \underline{\Gamma} && y = 0 \end{aligned} \tag{4}$$

Fig. 5 shows this schematically. The vorticity produced at the edge is transported downstream on the vortex sheet. The "leading edge" of the sheet must have a spiral shape, because of the presence of the discrete vortex Γ.

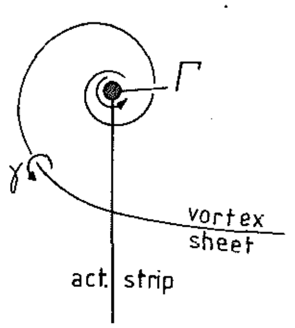

Fig. 5: Possible leading edge vortex sheet shape

Solution (4) is in agreement with (3): the type of singularity is the same; it is not complete however, as still the relation between $\underline{F}$ and $\underline{F}_e$, for given $\underline{u}_0$ is missing. Anyway, (4) can be used qualitatively. Momentum theory including these edge forces should show a shift of results towards a higher mass flow through the rotor. This momentum theory is already available, as it has been developed for augmented rotors (rotors with shrouds or tipvanes) by van Holten (ref. 4).

4. Momentum theory including edge forces

The extended momentum theory is not different from the classical theory in applying the conservation laws of mass, momentum and energy, but in the assumed force distribution. In the classical theory the total axial force, which of course is balanced by the change of momentum of the flow, equals the force doing work; in the present theory, there is a difference between these terms, as a part of the force distribution is normal to the local flow (so does not perform work) but still has an axial component.
Fig. 6 shows the streamtube, being used as control volume. The momentum balance reads

$$\tilde{F}_{ax} = F_{\Delta H}\ 2R + 2\tilde{F}_{e,ax} = \rho\ u_\infty\ (u_\infty - u_0)\ 2R_\infty \tag{5a}$$

Applying Bernoulli's law separately upstream and downstream of the strip shows:

$$F_{\Delta H} = \Delta H = {}^1\!/_2\,\rho\ (u_\infty{}^2 - u_0{}^2) \tag{5b}$$

*) Dutch National Aerospace Laboratory, Amsterdam.

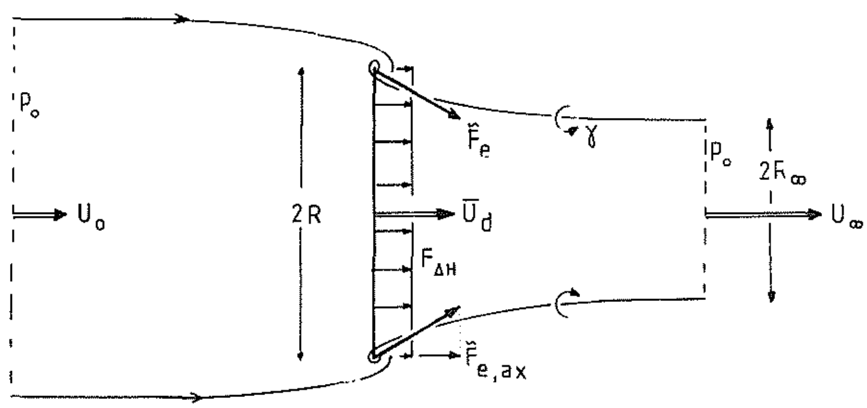

Fig. 6:
The control volume of the momentum theory.

while the mass balance simply is:

$$\bar{u}_d = u_\infty \frac{R_\infty}{R} \tag{5c}$$

The combination of (5a,b,c) with $\tilde{F}_e = 0$ gives the well-known result $\bar{u}_d={}^1/_2(u_0+u_\infty)$. Writing

$$\bar{u}_d = {}^1/_2\ (u_0+u_\infty) + \delta\bar{u}_d \tag{6a}$$

the "new" term $\delta\bar{u}_d$ appears to be connected to the edge forces:

$$\delta\bar{u}_d = \frac{\tilde{F}_{e,ax}}{\rho R}\ \frac{1}{(u_\infty-u_0)} = \frac{\tilde{F}_{e,ax}}{F_{\Delta H}R}\ \frac{(u_\infty+u_0)}{2} \tag{6b}$$

while

$$\bar{u}_d = \frac{\tilde{F}_{ax}}{\rho R}\ \frac{1}{2(u_\infty-u_0)} \tag{6c}$$

The power is:

$$P = F_{\Delta H}\ \bar{u}_d\ 2R \tag{6d}$$

The equations (6a,b,c,d) are the results of the momentum theory as developed by van Holten. $\delta\bar{u}_d$ is determined by the axial component of the edge force, and by the jump in total pressure $F_{\Delta H}$. The change of energy ΔH is not affected by $\underline{\tilde{F}}_e$: the work done per unit mass of flow remains the same, but the amount of mass is changed by assuming $\underline{\tilde{F}}_e \neq 0$. A positive $\delta\bar{u}_d$ supposes the axial component of $\underline{\tilde{F}}_e$ to have the same direction as $\underline{F}_{\Delta H}$. The radial component is not determined by the momentum theory. In fact the set of equations is incomplete: the relation between $\underline{F}_{\Delta H}$ and $\underline{\tilde{F}}_e$ is missing. Once this is known, a new performance curve for actuator strips, representing wind turbines and propellers, can be determined. A quantitative check is only possible if the missing relation is "loaned" from other calculations; this is done in the next section. A qualitative check shows that the results shift towards the dashed curve of fig. 2, if $\tilde{\underline{F}}_{e,ax}$ has the same direction as $\underline{F}_{\Delta H}$. This crucial condition is examined in section 6. If so, both the ideal induced power of a propeller as well as the ideal performance of a wind turbine will increase compared with the classical results.

5. The actuator strip in hover: a numerical comparison

Greenberg & Lee (ref. 2) published the results of their non-linear actuator strip calculations. For the hover state, $u_0=0$, the strength and shape of the vortex sheet is given, enabling a numerical comparison. The strength of the vortex sheet is given by a set of basic functions, one of these introducing the square-root singularity at the vortex sheet leading edge. This singularity is said to be dictated by the Green's function in the integral equation. This is not true: only if a (nearly) flat shape of the vortex sheet is assumed, the square-root singularity appears to be dictated. Furthermore, such a singularity (as present in a flat plate leading edge) is connected to an infinite or zero jump in pressure p or Bernoulli constant H: a finite jump, typically for the actuator strip vortex sheets, is impossible. Nevertheless, their model includes a singularity, and only in the near field of the edge, the difference will be noticeable. The edge force is determined as follows: taking the upper half plane as control volume for a momentum balance in y-direction, $\tilde{\underline{F}}_{e,radial}$ follows by:

$$\tilde{F}_{e,radial} = \int_{-\infty}^{+\infty} -(p-p_0)\ dx \tag{7}$$

As the velocity at the centerline is known, (7) can be calculated:

$$\tilde{F}_{e,radial} = -0{,}205\ {}^1/_2\rho u_\infty^{\,2} R \tag{8}$$

Fig. 7 shows the velocity and pressure distribution. If the classical actuator disc concept was valid ($\tilde{\underline{F}}_e = 0$), the pressure integral should be zero, due to an approximately antisymmetric distribution.
The direction of the force at the edge is normal to the local flow, which is normal to the tangent at the sheet near the singularity; with α as the angle between this tangent and the x-axis, the result is:

$$\tilde{F}_{ax} = \tilde{F}_{e,radial}\ \frac{1}{tg\alpha} = 0{,}09075\ {}^1/_2\rho u_\infty^{\,2}\ R \tag{9}$$

with $\alpha = 158{,}65^0$.

(6a,b), rewritten with u_0=0, then yield:

$$\frac{\bar{u}_d}{u_\infty} = \frac{1}{2} + \frac{\delta\bar{u}_d}{u_\infty} =$$

$$= \frac{1}{2}\left\{1 + \frac{\tilde{F}_{e,ax}}{{}^1\!/_2\,\rho u_\infty^2\;R}\right\} = 0{,}5454 \tag{10}$$

which agrees reasonably well with the result of Greenberg & Lee: u_d/u_∞ = 0,5535. The inset of fig. 3 shows this comparison.

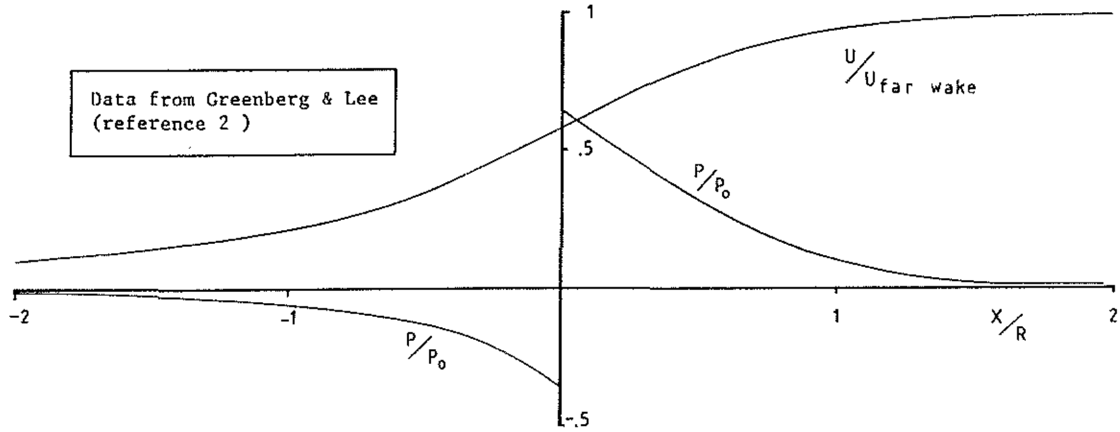

Fig. 7:
Velocity and pressure on the centerline of the actuator strip in hover.

6. The force distribution on real rotor blades

The previous chapters analysed the actuator strip, resulting in the determination of local forces $\underline{F}_n$, which are present in the momentum balance, but not in the energy (Bernoulli) equation. If the actuator strip is supposed to be a valid mathematical representation of a real rotor, these forces have to be present on a single rotor blade too.

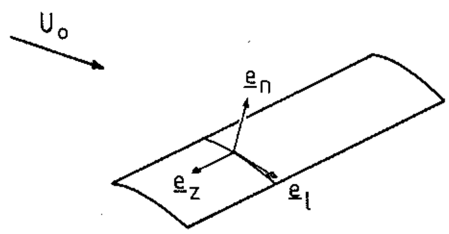

Fig. 8:
The lifting surface co-ordinate system.

Therefore the relation between forces and vorticity for a lifting surface is examined. Fig. 8 shows such a surface, consisting of a vortex sheet capable of sustaining a pressure jump. The sheet has thickness ϵ. As the other dimensions are finite, a free vortex sheet (not capable of carrying a load) is shed into the downstream flow. Using (1) with $\partial\underline{v}/\partial t$ = 0, the normal force F_n is obtained by integration across the thickness ϵ:

$$\underline{F}_n = \int_{-\epsilon/2}^{+\epsilon/2} \underline{f}_n \, h_n dn = \int_{-\epsilon/2}^{+\epsilon/2} \left[\underline{e}_n \frac{\partial H}{h_n \partial n} - \rho \, (\underline{v} \wedge \underline{\omega}) \right] h_n dn$$

$$= - \rho \int_{-\epsilon/2}^{+\epsilon/2} \underline{v} \wedge \underline{\omega} \, h_n dn \qquad (11)$$

Here h_n is the scale factor of the (z,l,n) system of fig. 8. z is the spanwise coordinate, l the chordwise coordinate. The normal velocity is assumed to be zero. For the limit $\epsilon \to 0$, (11) becomes a Dirac function integration, yielding:

$$\underline{F}_n = - \rho \, (\underline{v} \wedge \underline{\omega}) \, \epsilon = - \rho \, \underline{v} \wedge \underline{\gamma}$$

$$= \underline{e}_n \, \rho \, (v_l \gamma_z - v_z \gamma_l) \qquad (12)$$

The first term gives the local force on the bound vorticity γ_z, the second term (nominated as $\Delta \underline{F}_n$) the local force on the bound vorticity γ_l, see fig. 9. Usually this contribution to $\underline{F}_n$ is ignored, but for small aspect ratio's this isn't allowed. Kuchemann (ref. 6, page 163) shows measurements on a wing (aspect ratio 6) where this non-linear effect near the tips is clearly seen. Due to the strong asymmetry in rotor flow, the effective aspect ratio of a rotor blade is difficult to define. However, there is enough evidence that the tip vortex of a rotor blad induces high radial velocities near the tip, yielding significant v_z and γ_l values. Measurements of the blade load reported by Miller (ref. 7) show a high under pressure peak at the tip.

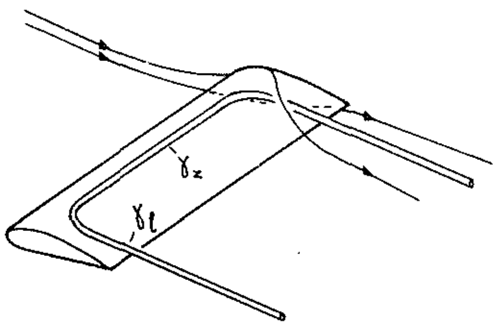

Fig. 9:
The occurrence of chordwise bound vorticity, experiencing a non-zero average spanwise velocity.

Calculations of Miller indeed show that such a peak is typical for an ideal load, instead of a constant load. It is easy to see that the first and second term of the right-hand side of (14) always have the same sign, as v_z is always directed inwards at the tip: $\Delta \underline{F}_n$ always increases the normal load.
In the momentum theory the rotor load is assumed to be distributed on the whole rotor disc. If the azimuthal velocities are neglected (only axial and radial velocities) the local axial rotor disc load is derived from (12):

$$\underline{F}_{ax} = \underline{e}_x \, \rho(-\Omega r \gamma_r - V_r \gamma_\phi) \qquad (13)$$

The power follows by the dot product of $\underline{F}_{ax}$ and the velocity $\underline{v}$: uF_{ax}. The second term on the right hand side (responsible for the high load on the outer annuli of the disc), contributes only little in the power: the mass flow through the outer annuli is very small. This shows the axial load appearing in the momentum balance, to differ appreciable from the axial load performing work.
This analysis has to be extended to the force system of one rotor blade (12), instead of a rotor disc consisting of an infinite number of blades (13).
The possible existence of tangential (radial) forces has to be included in this analysis. This will be done in ref. 8. Ref. 9 gives a physical description of the origin of the typical rotor force distribution.
An important result of this section is the determination of $\Delta\underline{F}_n$, having always the same orientation as the normal force on the bound spanwise vorticity.
This confirms the assumption of section 4, that the axial component of $\underline{F}_{edge}$ always has to have the same direction as the main load.

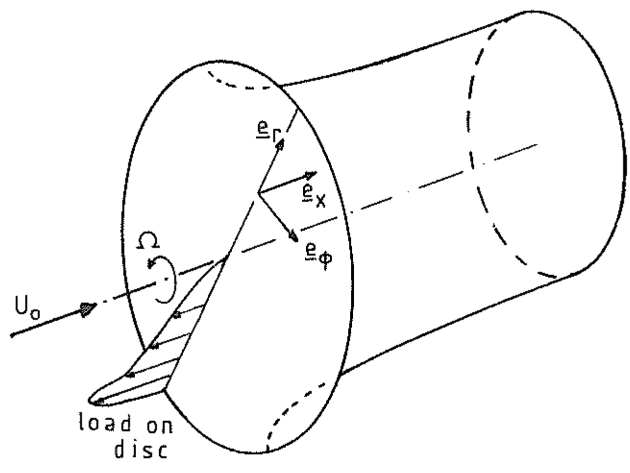

Fig. 10: The coordinate system of the rotor disc.

7. Conclusions

The classical actuator strip concept appears to be incomplete: the discrete edge forces, due to the vortex-flow singularity have to be added. The momentum theory including these forces is able to explain the systematic deviation of classical momentum theory results from experiments and non-linear calculations. For the hover case a quantitative confirmation has been obtained.
At the same time it has been shown that the force field of a real rotor blade exhibits the same essential feature: only a part of the axial load performs work while the total axial load changes the axial momentum of the flow.
Concerning the actuator strip analysis, the determination of the edge singularity has to be expanded to the actuator disc. With a non-linear calculation program including the edge singularity, the relation between disc load, velocity and edge force has to be determined. Then the extended momentum theory will provide a new ideal performance diagram for wind turbines and helicopter rotors.

References

1. F.W. Lanchester, A contribution to the theory of propulsion and the screw propeller, **Transactions of the Institution of Naval Architects**, volume 57, 1915.

2. M.D. Greenberg and J.H.W. Ree, Live momentum source in shallow, inviscid fluid, **Journal of Fluid Mechanics**, volume 145, 1984.

3. M.D. Greenberg, **Non-linear actuator disc theory, Zeitschrift fur Flugwissenschaften**, volume 3 no. 145, 1972.

4. Th. van Holten, Concentrator systems for wind energy, with emphasis on tipvanes, **Windengineering**, volume 5 no. 1, 1981.

5. G. Arfken, Mathematical methods for physicists, **Academic Press**, London, 1970.

6. D. Kuchemann, The aerodynamic design of aircraft, **Pergamon Press**, 1978.

7. R.H. Miller, A simplified approach to the free wake analysis of a hovering rotor, **Vertica**, volume 6, 1982.

8. G.A.M. van Kuik, Phd thesis, to appear in the course of 1988, Faculty of Physics, Eindhoven University of Technology.

9. G.A.M. van Kuik, The physics and mathematical description of the Achilles heel of stationary wind turbines aerodynamics: the tip flow, **Proceedings of the 6th European Wind Energy Conference**, Rome, October 1986.

10. F.S. Stoddard, Momentum theory and flow states for windmills, **Wind Technology Journal**, volume 1 no. 1, 1977.

11. W. Johnson, Helicopter Theory, **Princeton University Press**, Princeton New Yersey, 1980.

APPENDIX

The determination of the flow singularity at the half-infinite actuator strip.

The case with $\underline{u}_0 = 0$ (no parallel flow)

Fig. a1 shows a half-infinite actuator strip, thickness ϵ, with a force density distribution given by

$$\underline{f} = \underline{e}_x\, f_0\, \frac{1}{2}\left\{1 - \frac{y}{|y|}\left(\frac{y}{a}\right)^2\right\} \qquad |y| \le a$$

$$= \underline{e}_x\, f_0 \qquad y<a \qquad \text{(a-1)}$$

$$= \underline{e}_x\, 0 \qquad y>a$$

$\underline{f}$ is assumed to be a function of y only, for $|x| < {}^{\epsilon}/_{2}$, $\underline{f}$ is constant for a fixed y. Later on, the limit $a \to 0$ will be necessary; the distribution of $\underline{f}$ then becomes a Heaviside unit step function.

As only self-induced velocities are present, like in source/sink and vortex flows, circular symmetry is expected, by which $\underline{\nabla}x(\underline{v}x\underline{\omega}) = 0$ everywhere.
(2) then simplifies to:

$$\frac{1}{\rho}\, \underline{\nabla}\wedge\underline{f} = \frac{\partial}{\partial t}\,(\underline{\nabla}\wedge\underline{v}) \qquad \text{(a-2)}$$

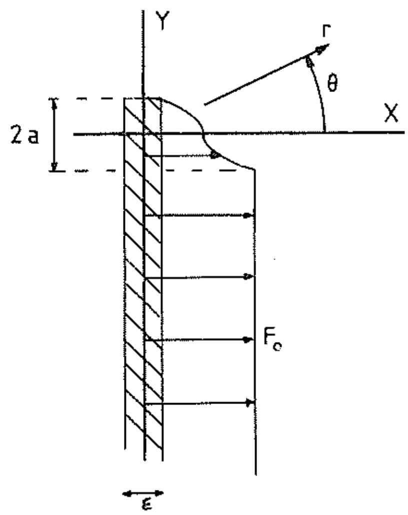

Fig. a-1: The half-infinite actuator strip, thickness ϵ, with $\underline{u}_0 = 0$.

By applying Gauss' theorem in the form (Arfken, ref. 5):

$$\iint_A \underline{\nabla}\wedge\underline{f}\, dA = \oint_s \underline{ds}\wedge\underline{f} \qquad \text{(a-3)}$$

with A the area of a circle, s the circumference of this, and $\underline{ds} = \underline{e}_n$ ds the outward normal vector on ds, (a-2) becomes after integration:

$$\frac{1}{\rho} \oint f \, ds = \frac{\partial}{\partial t} \oint v_\theta \, ds = \frac{\partial \Gamma}{\partial t} \qquad \text{(a-4)}$$

Now the limit $\epsilon \to 0$ is taken. The left-hand side of (a-4) then becomes:

$$- \frac{1}{\rho} \int_{-\epsilon/2}^{+\epsilon/2} f(y=r) \, dx + \frac{1}{\rho} \int_{-\epsilon/2}^{+\epsilon/2} f(y=-r) \, dx \qquad \text{(a-5)}$$

With (by definition):

$$\lim_{\epsilon \to 0} \int_{-\epsilon/2}^{+\epsilon/2} f_0 \, dx = F_0$$

substitution of (a-1) finally gives:

$$\begin{aligned} 2\pi r \, v_0(r,t) = \Gamma(r,t) &= \frac{F_0}{\rho} t & r \geq a \\ &= \frac{F_0}{\rho} \left(\frac{r}{a}\right)^2 t & r \leq a \end{aligned} \qquad \text{(a-6)}$$

(a-6) satisfies the assumption $\underline{\nabla} \times (\underline{v} \times \underline{\omega}) = 0$, so indeed is a solution of (2). It represents the well-known vortex with a "viscous core", see fig. a-2. For $a \to 0$, the F distribution becomes a step function, the resulting flow is that of the potential vortex, growing linearly in time.

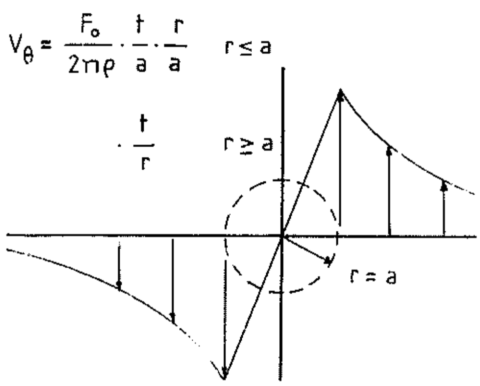

Fig. a-2:
The flow induced by the actuator strip of fig. a-1, with $\epsilon \to 0$.

The case with $U_0 \neq 0$

Suppose an element of an actuator strip, thickness ϵ, with an unknown force density distribution. The flow is assumed to be steady so (2) becomes:

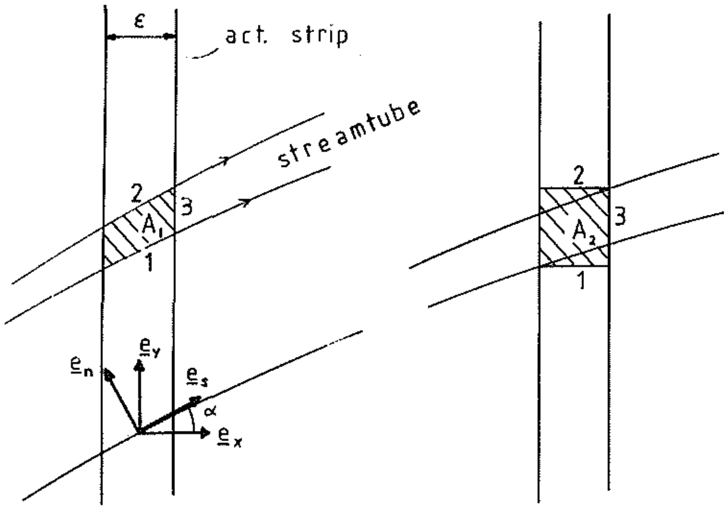

Fig. a-3:
The integration areas used in (a-8).

$$\frac{1}{\rho}\,\underline{\nabla}\wedge\underline{f} = -\,\underline{\nabla}\wedge(\underline{v}\wedge\underline{\omega}) \qquad \text{(a-7)}$$

With u and v as components of $\underline{v}$ in x and y direction (see fig. a-3), Gauss' theorem (a-3) applied to the surfaces A_1 and A_2 yields:

$$A_1: \quad \int_1 f_s\, h_s ds - \int_2 f_s\, h_s ds = \rho \int_3 u\omega\, dy$$

$$A_2: \quad \int_1 f_x\, dx - \int_2 f_x\, dx = \rho \int_3 u\omega\, dy \qquad \text{(a-8)}$$

$$+ \int_2 v\omega\, dx - \int_1 v\omega\, dx$$

h_s is the scale factor of the (s,n) coordinate system, fixed to the streamline; the indexes $_{x,y,s}$ denote: component in the direction of.
Per unit length (a-8) simplifies to:

$$\frac{d}{dy}\int_s f_s\, h_s ds = -\,\rho\,(u\omega)_{x=\epsilon/2}$$

$$\text{(a-9)}$$

$$\frac{d}{dy}\left[\int_x f_x\, dx - \int_s f_s\, h_s ds\right] = -\frac{d}{dy}\int_x \rho\, v\omega\, dx$$

If f_x, f_y are assumed to be a continuous function of y, development into a Taylor series around y_0 shows:

$$\int_s f_x(y)\ dx = \int_s f_x(y_0)\ dx + \int_s (y-y_0)\ \frac{df_x(y_0)}{dy}\ dx + \ldots$$

$$= \int_x f_x(y_0)\ dx + \int_s (y-y_0)\ \frac{df_x(y_0)}{dy}\ dx + \ldots \qquad \text{(a-10)}$$

For $\epsilon \to 0$, only the first term remains.

Furthermore, $\int_s f_s\ h_s ds$ can be written as:

$$\int_s f_s\ h_s ds = \int_s f_x\ dx + \int_s f_y\ dy$$

$$= \int_s f_x\ dx + \int_s f_y\ tg\alpha\ dx \qquad \text{(a-11)}$$

by which, for $\epsilon \to 0$, the left-hand side of (a-9) is:

$$\frac{d}{dy}\left[\int_x f_x\ dx - \int_s f_x\ dx - \int_s f_y\ tg\alpha\ dx\right]$$

$$= \frac{d}{dy}\left[-\int_x f_y\ tg\alpha\ dx\right] \qquad \text{(a-12)}$$

Using (a-10), (a-12) combined with (a-9) gives the resultant forces for $\epsilon \to 0$:

$$\lim_{\epsilon \to 0} \int_x f_y\ tg\alpha\ dx = \lim_{\epsilon \to 0} \int_x \rho\ v\omega\ dx + C_1$$

$$\lim_{\epsilon \to 0} \int_x f_x\ dx = \lim_{\epsilon \to 0} \left[\int_s f_s\ h_s ds - \int_x \rho\ v\omega\ dx\right] + C_2 \qquad \text{(a-13)}$$

All integrations become integrations of functions of the Dirac and Heaviside type. $tg\alpha$ then may be transported to the right hand side with which F_y becomes (omitting C_1):

$$F_y = \lim_{\epsilon \to 0} \int_x f_y \, dx = \lim_{\epsilon \to 0} \int_x \rho \, u\omega \, dx \tag{a-14}$$

The expression for F_x contains $\int f_s \, h_s ds$.

By (1) it is clear that:

$$\int_s f_s \, h_s ds = \Delta H \tag{a-15}$$

with ΔH the increase of the Bernoulli constant on passing the strip.
(a-15) substituted in (a-13) gives for F_x:

$$F_x = \lim_{\epsilon \to 0} \int_x f_x \, dx = \Delta H - \lim_{\epsilon \to 0} \int_x \rho \, v\omega \, dx \tag{a-16}$$

(a-14) and (a-16) give the forces for any actuator strip with zero thickness, in relation to u,v and ω. A more clarifying expression is:

$$\left.\begin{aligned} \overline{F}_{\Delta H} &= \underline{e}_x \, \Delta H = \lim_{\epsilon \to 0} \underline{e}_x \int_s f_s \, h_s ds \\ \underline{F}_n &= \lim_{\epsilon \to 0} \int_x - \rho \, (\underline{v} \wedge \underline{\omega}) \, dx \end{aligned}\right\} \tag{a-17}$$

(a-17) shows that any distribution of $\underline{F}_{\Delta H}$, the force which does work (it changes H), is accompagnied by $\underline{F}_n$, when at the same time vorticity is produced at the strip.
F_n is perpendicular to the local flow, so does not perform work.
$\underline{F}_{\Delta H}$ can be considered as an independent variable, $\underline{F}_n$ as a dependent. If $\underline{F}_{\Delta H}$ is assumed to be distributed as (a-1), the strip with constant load $\underline{F}_{\Delta H}$ is achieved by the limit $a \to 0$. The discrete force $\tilde{\underline{F}}_n$ follows by integration of $\underline{F}_n$ in y-direction:

$$\tilde{\underline{F}}_{n,edge} = \lim_{\substack{\epsilon \to 0 \\ a \to 0}} \int_x \int_y - \rho \, (\underline{v} \wedge \underline{\omega}) \, dxdy \tag{a-18}$$

This is an integration of a Dirac function in x and y, yielding with A as edge "surface":

$$\tilde{\underline{F}}_{n,edge} = - \rho \, (\underline{v} \wedge \underline{\omega}) \, A = - \rho \, \underline{v} \wedge \underline{\Gamma}_{edge} \tag{a-19}$$

Apparently, an actuator strip with constant load $\underline{F}_{\Delta H}$, creates a flow singularity at the edges, the type of which is a discrete vortex. This vortex acts as the leading edge of the vortex sheet springing from the edge. This sheet is characterized by the same jump in H as the strip itself:

$$\Delta H_{sheet} = | \underline{F}_{\Delta H} | = \Delta \left({}^{1}/_{2} \rho \underline{V} \cdot \underline{V} \right)$$

$$= \rho \, v_s \, \gamma \qquad \text{(a-20)}$$

where v_s is the sheet velocity, being the average of the velocities on both sides, and γ is the difference in velocities. The edge flow is determined completely if the shape and strength of the sheet is known, taking (a-19) into account.